Solid State Phenomena
ISSN: 1662-9779, Vol. 375, pp 35-41
doi:10.4028/p-I5U9fS

Submitted: 2024-09-21
Revised: 2025-08-08
Accepted: 2025-08-08
Online: 2025-09-05

Formation Mechanism and Complex Faulting Behavior of a BPD Loop in 180 µm Thick 4H-SiC Epitaxial Layer

Zeyu Chen[1,a *], Nadeemullah A. Mahadik[2,b], Michael Dudley[1,c], Balaji Raghothamachar[1,d], David A. Scheiman[2,e], Robert E. Stahlbush[2,f], Youngsang Kim[3,g] and Michael. W. Owen[3,h]

[1]Department of Materials Science & Chemical Engineering, Stony Brook University, Stony Brook, NY 11794 USA

[2]US Naval Research Laboratory, Washington, DC, 20375, USA

[3]Defense Microelectronics Activity, McClellan Park, CA 95652

[a]zeyu.chen@stonybrook.edu, [b]nadeem.mahadik@nrl.navy.mil, [c]michael.dudley@stonybrook.edu, [d]balaji.raghothamachar@stonybrook.edu, [e]david.a.scheiman2.civ@us.navy.mil, [f]robert.e.stahlbush.civ@us.navy.mil, [g]youngsang.kim4.civ@mail.mil, [h]michael.w.owen.civ@mail.mil

Keywords: 4H-SiC; Stacking Fault; Partial Dislocation dipole; UV Photoluminescence Imaging; X-ray Topography

Abstract. 4H-SiC with 180 µm epilayer was subjected to UV exposure. Stacking fault expanded from basal plane dislocation (BPD) loop generated during growth in the epilayer was observed by UV Photoluminescence Imaging (UVPL) and X-ray Topograph (XRT) techniques. Interactions between partial dislocation, emanating from the BPD loop and gliding via recombination-enhanced dislocation glide mechanism, and threading screw/mix dislocations are detected and analyzed, where stacking faults migrate to different basal plane after the interactions. Such migration increases the faulted volume that can severely degrade reliability and performance of high power SiC devices by increasing reverse leakage current and on-state resistance and could eventually lead to device failure.

Introduction

Silicon Carbide (SiC) is a wide bandgap semiconductor with considerable potential for power devices due to its high breakdown field and excellent thermal conductivity. These properties enable SiC devices to function effectively under extreme conditions, including high temperatures, voltages, and frequencies [1]. Currently, commercially available devices can handle voltages up to 3.3kV and are primarily used in automotive and traction control applications. However, there is a need for SiC devices with higher voltage ratings (>6.5kV) for use in hybrid systems, shipboard power, grid systems, and defense applications. To achieve the required breakdown voltages, these devices are manufactured on SiC wafers with thick epitaxial layers [2]. As the thickness of the epitaxial layer increases, the density of defects formed during growth also rises [3], which can significantly impact device performance. Recent research by Mahadik et al. has identified a complex stacking fault originating from the substrate and extending into a 180 µm thick epitaxial layer. This fault generates several Shockley-type stacking faults (SSFs) when carriers are injected via UV excitation, through a recombination-enhanced dislocation glide mechanism [4,5,6]. Such stacking faults are detrimental to the device performance, causing decrease of forward voltage during on-state and increase of leakage current during off state.

Additionally, another defect commonly observed in epitaxial layers is the interfacial dislocation (ID) accompanied by half-loop arrays (HLAs) [7]. These HLAs form when screw-oriented basal plane dislocations (BPDs) glide under mismatch stresses, causing bending at the growth front and leading to their conversion into threading edge dislocations (TEDs). When the gliding velocity of BPDs surpasses the growth rate of the epitaxial layer, some of these dislocations protrude through the surface, creating HLAs composed of two TEDs and a segment of BPD that can dissociate into

stacking fault bounded with partial dislocations as well [8]. Therefore, generation of BPDs and SSFs are the major impedances for developing high voltage bipolar devices such as insulated gate bipolar transistors, and they should be carefully characterized and investigated. In this paper, 4H-SiC with 180 μm epilayer was characterized by ultraviolet photoluminescence (UVPL) imaging and High-resolution X-ray topography (XRT). Interaction between threading screw/mixed dislocations and partial dislocation generated from BPD loop during UV excitation was observed and analyzed.

Experiment

4H-SiC with 180 μm epilayer doped with $2x10^{14}$ cm^{-2} n-type was subject to whole wafer UVPL imaging [9], using a 4 Watt, 355 nm UV laser that was coupled to a custom microscope with automated high precision XYZ stage. UVPL images were acquired with 2 μm spatial resolution, using a 665 nm long pass emission filter, and a liquid N2 cooled CCD detector and sequential images were acquired with 1 μm spatial resolution on the selected SSF.

High-resolution x-ray topography (XRT) was performed using a Rigaku XRTMicron system equipped with a 70 μm micro-focus, 1.2kW Cu/Mo rotating anode. The system has a vertical 3-circle goniometer with up to 200 mm diameter sample stage, and a 2.2 μm pixel x-ray camera. XRT image of the complex defect was acquired using **g** = [11-20] in transmission geometry with MoKα radiation.

Results and Discussion

Fig. 1(a) shows 11-20 XRT image before UV exposure, where a screw BPD (**b**=1/3[11-20]) originating from the substrate is replicated into the epilayer forming a BPD loop and ID. However, no HLA is observed associated with the ID. The formation mechanism of such defect is that the screw BPD segment first get replicated into epilayer (Fig. 1(b)) then glides under the misfit stress (Fig. 1(c)). Due to the change in the line direction, the BPD segment at the growth front will deviate from screw type allowing the that the partials to constrict enabling conversion to TED which now acts as a pinning point (Fig. 1(d)). In this case, differing from the formation of HLAs, the relative gliding speed of the BPD is lower than the growth rate of the epilayer due to lower stress, so it propagates as a loop in the epi-layer and forms ID at the epi/sub interface (Fig. 1(e) and 1(f)). Such a BPD loop in the epilayer acts as a single-ended Frank Read source. As the loop expands in the epilayer encounters TSD/TMDs, segments of the BPD loop will migrate to different basal planes via the jog mechanism [10]. Upon UV excitation, stacking faults and partial dislocations will expand from this looping BPD segment on different basal planes. When opposite sign partial dislocations which have same Burgers vectors and opposite line directions located on different basal planes and align on top of each other along [0001] direction, partial dislocation dipole (PDD) can be formed [11], due to the attractive force between the opposite sign partial dislocations. Fig. 2 shows UVPL images (2D projections of 3D microstructure) indicated by the red box, where the red number indicates the basal plane the stacking faults are located on, and the corresponding 3D schematic of the mechanism of interactions between partial dislocations and TSD/TMDs (indicated by the yellow arrows in UVPL image of Fig. 2(b)). In this figure, a total of 4 basal planes (labeled at bottom left corner on each plane) and three TSD/TMDs are involved. TMD1 and TMD3 are assumed to be right-handed with Burgers vector of the screw component of $[0001]$ and TMD2 is left-handed with Burgers vector of the screw component of $[000\bar{1}]$. When the stacking fault bounded by partial dislocation interacts with right-handed screw TMD, the left side of the fault will stay on the same plane while the right side of the fault will advance to the plane above with respect to the advancing direction due to the to the helical shape with clockwise orientation. On the other hand, if such a fault interacts with left-handed TMD, the left side of the fault remains on the same plane, while the right side of the fault will move to the plane below.

At the start of UV illumination, two double rhombic shape SFF on plane 2 and 4, and a PDD1 are formed due to UV excitation as highlighted in the UVPL image by the red arrow and the red segment in the 3D diagram in Fig. 2(a). Si-core partials with Burgers vector 1/3$[01\bar{1}0]$ [12] are labeled as P1 to P3, where P1 and P3 will advance along $[1\bar{1}00]$, and P2 and P4 will advance along $[11\bar{2}0]$ upon UV excitation. When P3 advances and interacts with TMD1, resulting in the left side of the fault with P3-2 segment remaining on plane 4 and the right side of the fault with P3-1 segment advancing to plane 3 and forming PDD2 illustrated by the orange solid lines, as shown in Fig.2 (b). As P2 advance to the right and P3-2 propagate along $[1\bar{1}00]$, the partials belonging to PDD1 and PDD2 on plane 4 are elongated and shorten P3-2 segment until it disappears. In addition, as P2 propagating to the right encounters the advancing P3-1 toward $[1\bar{1}00]$, PDD3 is formed, as shown in Fig.2 (c). After that, P1 keep advancing and then the elongated P2 propagates to the right and interacts with TMD3, resulting in the left side of the fault, with respect to the advancing direction, staying on plane 2 having P2-1 segment and the right side moves to the plane 1 with P2-2 segment, forming PDD4 composed of PDD4-1 and PDD4-2 and indicated by yellow solid line in the 3D schematic.

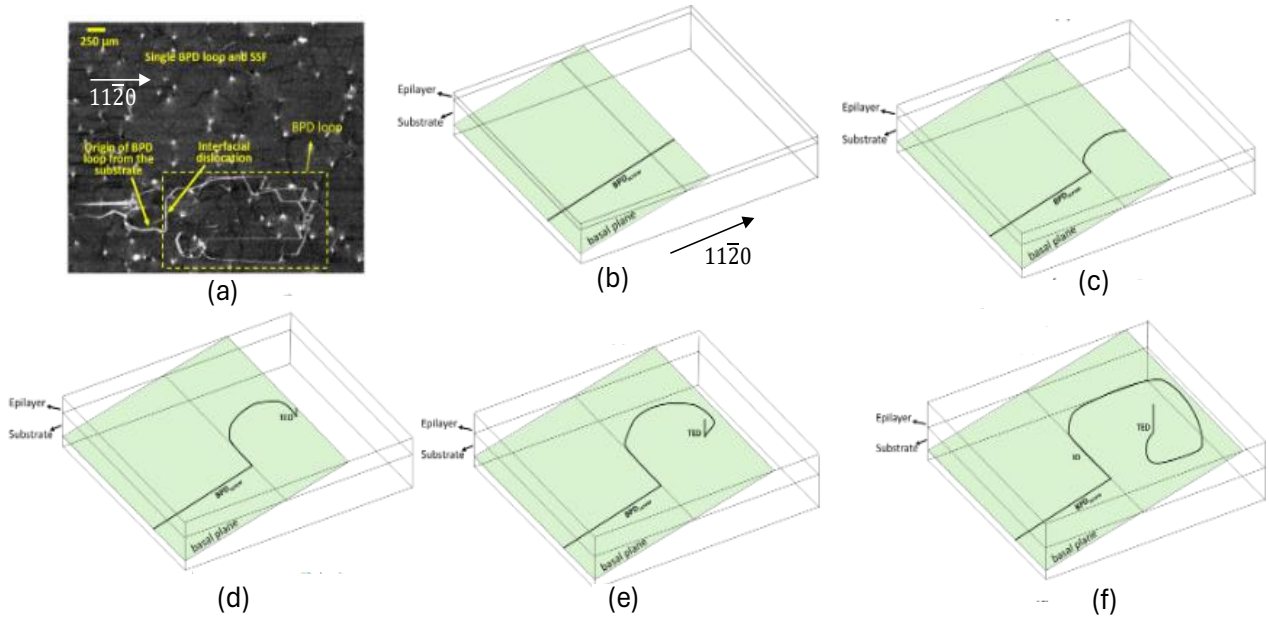

Fig. 1. (a) High resolution 11-20 XRT image of formation of BPD loop and ID in epilayer due to the original BPD in substrate. (b) to (f) Schematic of formation mechanism of the BPD loop and ID in epilayer.

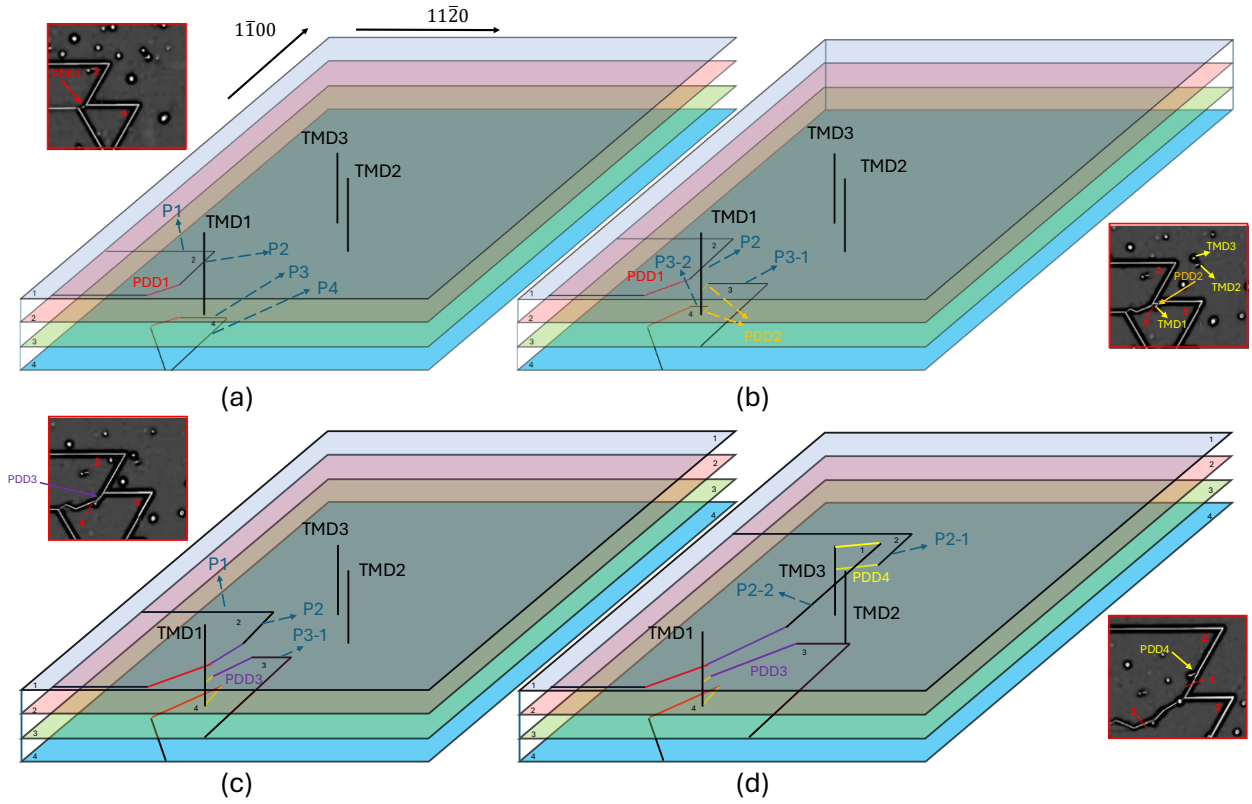

Fig. 2. (a)-(d) 3D schematic of propagation of partial dislocations of the SSFs interacting with TMD1 and TMD3 forming PDD1 to PDD4, where the black numbers in the images indicate the corresponding basal planes of the SSFs are located at. UVPL images are shown in the red boxes, where the red numbers in the images indicate the corresponding basal planes of the SSFs located at.

Then, P2-2 segment interacts with TMD2 with Burgers vector of the screw component of $[000\bar{1}]$, leading to the left side of the fault with P2-2 segment staying on plane 1 and the right side of the fault with P2-3 segment advancing to plane 2 and forming PDD5, as shown in Fig.3 (a). In addition, a stacking fault on plane 2 expands from the lower part of the crystal as indicated by the green arrows in the 3D schematic and UVPL image. Fig 3(b) indicates movement of the Si-core partials, where PDD3 gets elongated with shortening of P2-3 segment and approaches PDD5. As PDD3 reaches the vicinity of PDD5-1 (shown in Fig.3 (b)), PDD3-1 and PDD3-2 can be disrupted. The interaction force of 9.12 GPa between the screw component of partials of PDD3 can be estimated by the force between screw dislocations (Eq.1) [13] since the line direction is almost parallel to Burgers vector:

$$F_r = \frac{Gb^2}{2\pi r} \tag{1}$$

Where G is the shear modulus, b is the Burgers vector and r is the distance between the dislocation. The glide force acting due to the partial of PDD5 on plane 1 on PDD3 can be calculated by Eq.2 [14,15]:

$$F_g = \frac{Gb_1b_2 \sin 2\theta}{4\pi(1-v)h}[-\sin^2\lambda\,(\cos 2\theta) + \cos^2\lambda\,(1-v)] \tag{2}$$

Where b_1 and b_2 are Burgers vector of the two dislocations, h is the shortest distance between the dislocations, v is the Poisson's ratio, λ is the angle between line direction and b_1, and θ can be described as $\tan^{-1}(\frac{h}{a})$, where a is arbitrary length along dislocation with b_1. In this case, partial of PDD5-1 will be dislocation with b_1, as shown in Fig. 4(a). The maximum force that PDD5-1 acts on PDD3-1 is 3.6 GPa and 1.8 GPa on PDD3-2 along the opposite direction since they are opposite sign

pairs, as shown in Fig. 4(b), which is equivalent to PPD3-1 subjected to total force of 5.4 GPa. Next, resolved force from force between screw dislocations is calculated. As shown in Fig. 4(c), the resolved force (F_a) can be calculated by the following equation modified from Eq.1:

$$F_a = \frac{Gb^2 \cos\alpha}{2\pi \frac{d}{\sin\alpha}} \tag{3}$$

where α is the angle between force of screw component (F_r) and resolved force (F_a), and d is the distance between the dipole along [0001] direction. Based on Eq.3, the maximum resolved force on PDD3-1 is around 4.4 GPa, which is smaller than the 5.4 GPa force acting from PDD5-1 on PDD3-1. Therefore, the dipole is broken up, and dislocation then migrates to the position having lowest Peierls barrier, where line direction of dislocation is parallel to $[11\bar{2}0]$. Fig. 3(c) shows the 3D schematic after PDD3 has been decomposed, where PDD3-1 will move to the right and PDD3-2 will move to the left, and as PDD3-2 expand, it will interact with TMD2, where the left side of the fault will stay on plane 3 and right side will move to plane 4, rearranging the PDD5-1 and partial on plane 4 to form PDD6. As P5 advances to the right, PDD7 is formed with the partial on plane 2 and 3. Then P6 propagates and interacts with TMD1, where the left side will stay on plane 3. The right side of P6 (P6-2 in Fig. 3(d)) will attract PDD 4-2 to form PDD8, since PDD4-2 will subject to equal but opposite sign force from PDD4-1 and P6-2, and the Si-core PDD4-1 tend to propagate due to UVPL excitation and the PDD4-2 tend to form dipole with P6-2 along $[11\bar{2}0]$ with lower Peierls barrier, leading to rearrangement of dipole and formation of PDD8. In addition, as PDD4-1 and P6-1 advanced, PDD9 will form, as indicated in Fig. 3(d).

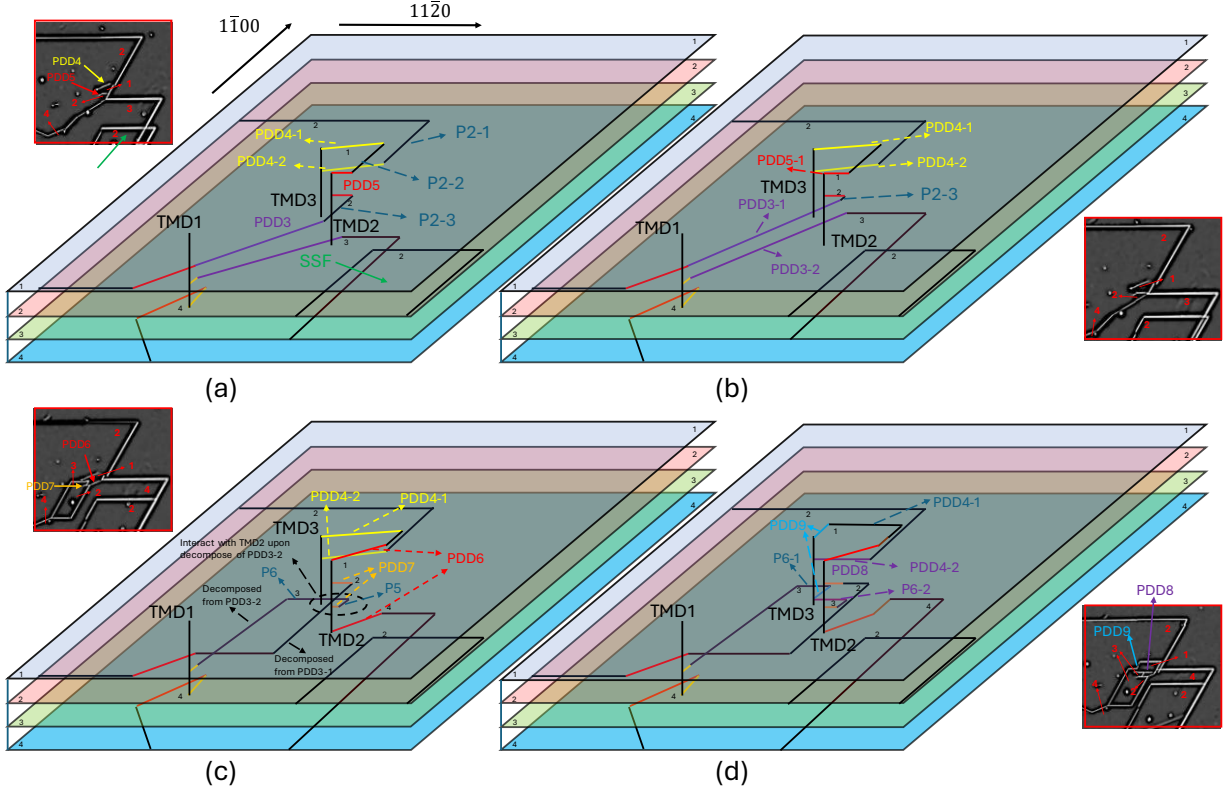

Fig. 3. (a) and (b) 3D schematic of propagation of partial dislocations of the SSFs interact with TMD2 and TMD3 forming PDD5, (c) and (d) schematic showing decomposition of PDD3, and the segment decomposed from PDD3-2 interact with TMD3 .

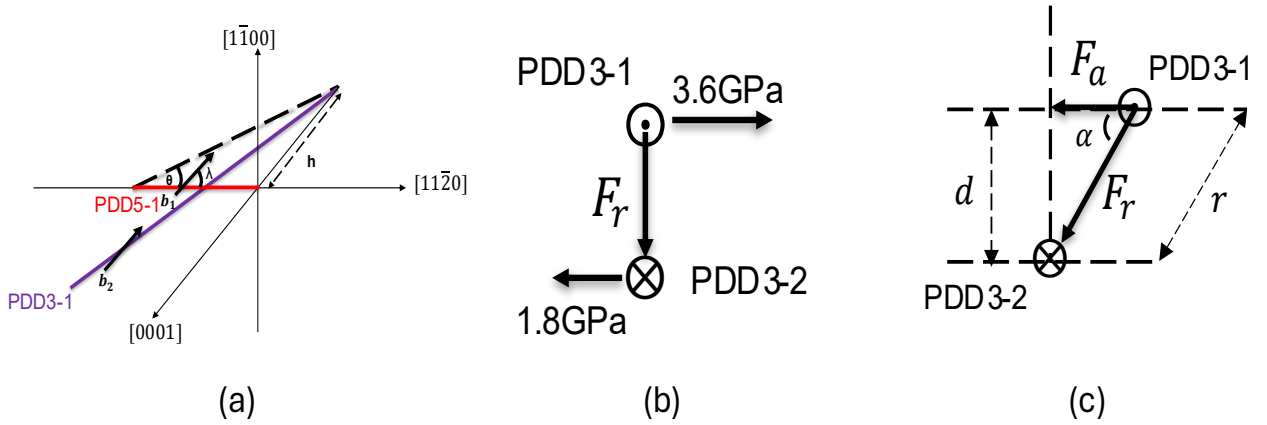

Fig. 4. (a) Schematic diagram for interaction force of PDD5-1 acting on PDD3-1. (b) Force on PDD3-1 and PDD3-2 subjected by PDD5-1. (c) Force analysis while PDD3-1 and PDD3-2 separate.

The SSF originating from lower part of the crystal expands to the vicinity of the partial separated from PDD3-1 (Fig. 5(a)), then the opposite sign partials get annihilated as highlighted in yellow solid line box and the two SSFs merge. Then, P7 from the merged SSF approaches PDD4-2, changing the line direction of PDD7-1, and the line direction of PDD7-2 will follow due to the attraction force between the dipole, as shown in Fig. 5(b). When P7 encounters PDD4-2, part of the partials will get annihilated (yellow dashed box in Fig. 5(b)), then the two faults will merge together and the dislocation segments will join together, as shown in Fig. 5(c). After that, P8 will advance to the right as P7 shortens in length (Fig. 5(d), until it reaches the surface as indicated in the UVPL image of Fig. 5(d).

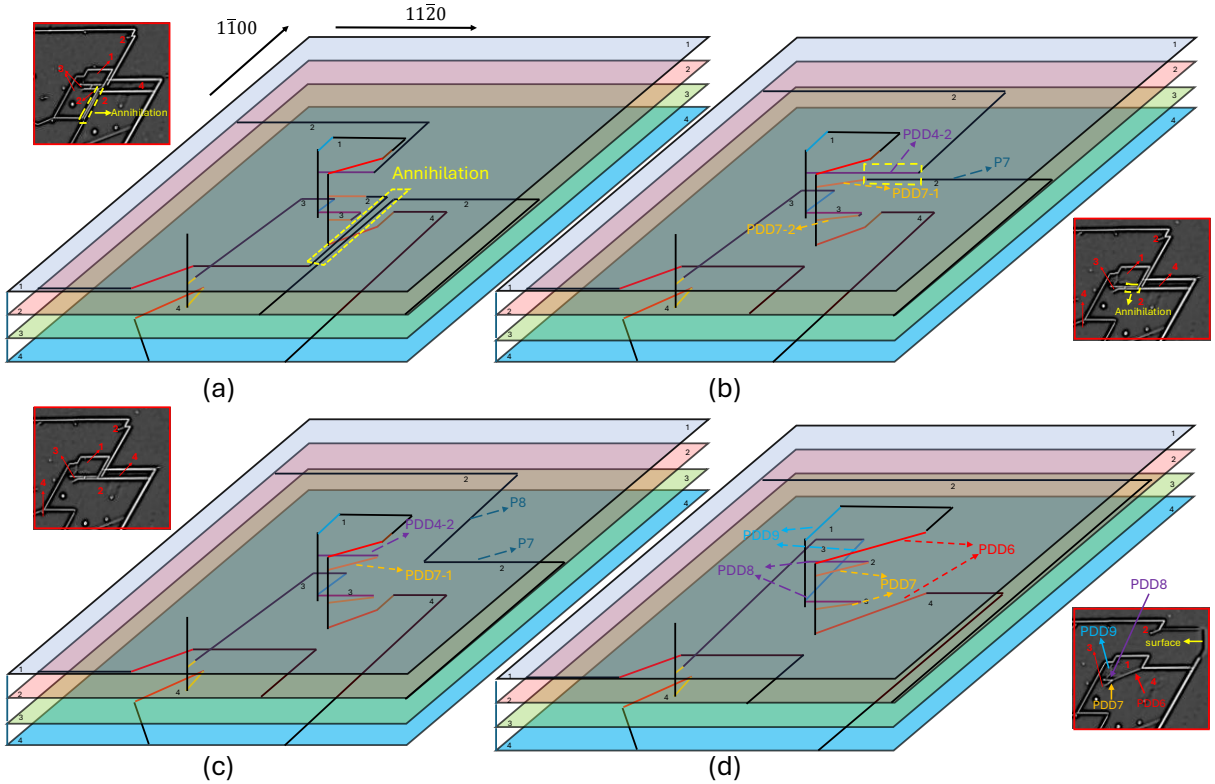

Fig. 5. (a) and (b) two annihilation processes of opposite sign partials on plane 2, leading to three different SSFs on plane 2 merging into one. (c) after annihilation processes, PDD7-1 join PDD4-2 while P8 keeps migrating to the right as P7 shortens. (d) the migration of P8 stops at the surface, while PDD6 to PDD9 remain in the epilayer.

Summary

The formation of a dislocation loop with associated interfacial dislocation during thick 4H-SiC epilayer growth has been observed. Different portions of the loop can migrate to different basal planes via interaction with TMDs during epilayer growth. Upon UV excitation, different portions of the loop expand and form SSFs. Complex mechanisms for interaction between SSFs and TMDs upon UV excitation have been analyzed and explained with 3D schematic diagrams. When SSF interacts with TMD, the fault will be separated in adjacent basal planes leading to formation of partial dislocation dipoles. Dipole-dipole interactions, including rearrangement, separation and annihilation, are observed and reported. The interactions and expansion of SSFs can severely degrade the device performance and reliability of high power SiC devices by increasing reverse leakage current and on-state resistance, which could eventually lead to device failure.

Acknowledgement

The information, data, or work presented herein was funded in part by the Advanced Research Projects Agency-Energy (ARPA-E), U.S. Department of Energy, under Award Number DE-AR0001028. The views and opinions of authors expressed herein do not necessarily state or reflect those of the United States Government or any agency thereof.

References

[1] A.A. Lebedev and V.E. Chelnokov, Semiconductors 33, 999–1001 (1999).

[2] P. Luo and S. N. E. Madathil, IEEE Transactions on Electron Devices, 67 5621-5627 (2020)

[3] H. Tsuchida, I. Kamata, T. Miyazawa, M. Ito, X. Zhang and M. Nagano, Materials Science in Semiconductor Processing, 78, 2 (2018)

[4] N. A. Mahadik, R.E. Stahlbush, M. Dudley, B. Raghothamachar, M. Hinojosa, A. Lelis and W. Sung, Scripta Materialia 235, 115598 (2023)

[5] J.P. Bergman, H. Lendenmann, PA. Nilsson, U. Lindefelt and P. Skytt ., Mater. Sci. Forum 353–356, 299–302 (2001)

[6] A. Galeckas, J. Linnros and P. Pirouz, Appl. Phys. Lett. 81, 883–885 (2002)

[7] N. Zhang, Y. Chen, Y. Zhang, M. Dudley and R. E. Stahlbush, Appl. Phys. Lett. 94, 122108 (2009)

[8] N. A. Mahadik, R. E. Stahlbush and W. Sung, J. Appl. Phys. 131, 225702 (2022)

[9] R. E. Stahlbush, K. X. Liu, Q. Zhang, and J. J. Sumakeris, Mater. Sci. Forum 556-557, 295 (2007)

[10] D. Hull and D.J. Bacon, Intersection of Dislocations, in: Fifth Edition, Introduction to Dislocations, Elsevier, 2011, pp.137-139.

[11] Y. Chen, M. Dudley, K. X. Liu, R. E. Stahlbush, Appl. Phys. Lett. 90, 171930, (2007)

[12] A. Iijima, I. Kamata, H. Tsuchida, J. Suda and T. Kimoto, Philosophical Magazine,97:30, 2736-2752, (2017), DOI:10.1080/14786435.2017.1350788

[13] D. Hull and D.J. Bacon, Intersection of Dislocations, in: Fifth Edition, Introduction to Dislocations, Elsevier, 2011, pp.75-79.

[14] C. S. Hartley, and J. P. Hirth, Acta Metallurgica 13.2 79-88. (1965)

[15] D. Caillard, Modelling and Simulation in Materials Science and Engineering 32.3: 035027. (2024)